JACS
JOURNAL OF THE AMERICAN CHEMICAL SOCIETY

Communication

pubs.acs.org/JACS

Robust Nonenzymatic Hybrid Nanoelectrocatalysts for Signal Amplification toward Ultrasensitive Electrochemical Cytosensing

Tingting Zheng,[†,‡] Qingfeng Zhang,[†] Sheng Feng,[†] Jun-Jie Zhu,*[,‡] Qian Wang,[†] and Hui Wang*[,†]

[†]Department of Chemistry and Biochemistry, University of South Carolina, Columbia, South Carolina 29208, United States

[‡]State Key Laboratory of Analytical Chemistry for Life Science, School of Chemistry and Chemical Engineering, Nanjing University, Nanjing, Jiangsu 210093, China

Supporting Information

ABSTRACT: We have discovered that magnetic Fe_3O_4 nanoparticles exhibit an intrinsic catalytic activity toward the electrochemical reduction of small dye molecules. Metallic nanocages, which act as efficient signal amplifiers, can be attached to the surface of Fe_3O_4 beads to further enhance the catalytic electrochemical signals. The Fe_3O_4@nanocage core–satellite hybrid nanoparticles show significantly more robust electrocatalytic activities than the enzymatic peroxidase/H_2O_2 system. We have further demonstrated that these nonenzymatic nanoelectrocatalysts can be used as signal-amplifying nanoprobes for ultrasensitive electrochemical cytosensing.

Developing highly robust and efficient electrocatalysts is of key importance to the optimization of the performance of fuel cells[1,2] and electrochemical biosensors.[3,4] A variety of metallic,[5,6] nonmetallic,[7] and hybrid nanostructures[8,9] have shown intriguing electrocatalytic activities with great potential to be implemented into fuel cells. For electrochemical biosensing, the detection sensitivity can be significantly improved by using specifically designed electrocatalysts for signal amplification. A widely used strategy for signal amplification is to load natural enzymes, such as peroxidase,[10−14] glucose oxidase,[15,16] and alkaline phosphatase,[17] onto electrodes or nanocarriers to enhance the detection sensitivity through enzymatic electrochemical processes. However, enzymes are vulnerable to proteolytic degradation, and their native conformations can be easily disrupted by even slight changes in the environment, resulting in the loss of their catalytic activities. In addition, the preparation, purification, and storage of enzymes are time-consuming and expensive. Therefore, robust nonenzymatic nanoelectrocatalysts with high catalytic efficiencies are highly desirable.

Magnetic Fe_3O_4 nanoparticles (NPs) have widespread biomedical applications in biological sample separation, therapeutic drug delivery, and magnetic resonance imaging.[18] In 2007, it was discovered that Fe_3O_4 NPs in the size regime from tens of nanometers to submicrometers possess an intrinsic enzyme-mimicking activity similar to that of natural horseradish peroxidase (HRP).[19] Since then, a variety of Fe_3O_4-containing nanocomposites have been found to be catalytically active toward the chemical or electrochemical reduction of H_2O_2.[20−23] Here we report a surprising discovery that Fe_3O_4 beads exhibit intrinsic electrocatalytic activities toward the electrochemical reduction of small dye molecules even in the absence of H_2O_2. The catalytic electrochemical signals can be further amplified by assembling metallic nanocages on the surface of the Fe_3O_4 beads.

The hybrid nanoelectrocatalysts were prepared through a layer-by-layer assembly process, as schematically illustrated in Figure 1A. Ag–Pd bimetallic nanocages were synthesized through galvanic replacement reactions using Ag nanocubes[24] (see Figure S1 in the Supporting Information) as the sacrificial templates.[25] Submicrometer polycrystalline beads composed of Fe_3O_4 nanocrystals were prepared using a previously reported

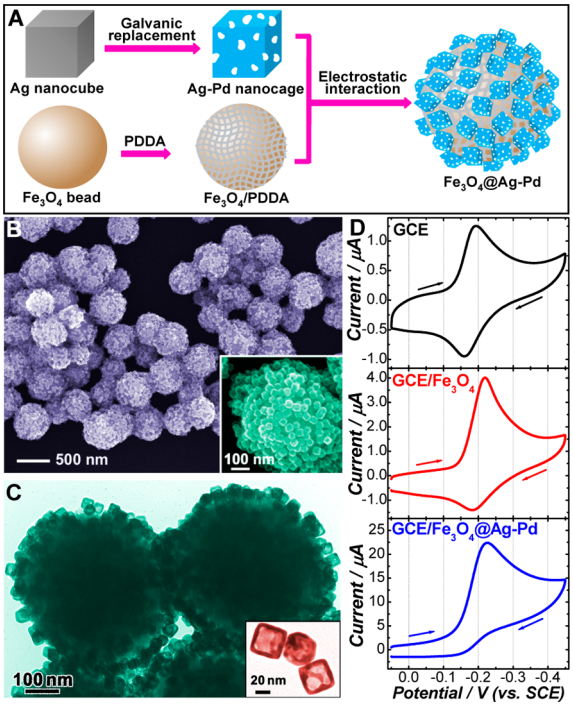

Figure 1. (A) Schematic illustration of the fabrication of Fe_3O_4@Ag–Pd hybrid NPs. (B) SEM image of Fe_3O_4@Ag–Pd hybrid NPs. The inset highlights one Fe_3O_4@Ag–Pd hybrid particle. (C) TEM image of Fe_3O_4@Ag–Pd hybrid NPs. The inset shows a TEM image of Ag–Pd nanocages. (D) CVs of a bare GCE, GCE/Fe_3O_4, and GCE/Fe_3O_4@Ag–Pd in 0.01 M PBS buffer (pH 7.0) containing 25 μM thionine. Scan rate = 50 mV s^{-1}.

Received: January 7, 2014
Published: January 27, 2014

 © 2014 American Chemical Society dx.doi.org/10.1021/ja500169y | J. Am. Chem. Soc. 2014, 136, 2288−2291

microwave-assisted solvothermal method[26] with minor modifications. The surfaces of the Fe_3O_4 beads were terminated by carboxyl groups and thus were negatively charged at neutral pH (Figure S2). The adsorption of positively charged poly(diallyldimethyl ammonium chloride) (PDDA) on colloidal Fe_3O_4 beads switched the ζ potential to a positive value. Ag−Pd nanocages with negatively charged surfaces were subsequently tethered electrostatically to the surface of the Fe_3O_4/PDDA particles. As shown by the scanning electron microscopy (SEM) and transmission electron microscopy (TEM) images in Figure 1B,C, respectively, a submonolayer of uniformly distributed Ag−Pd nanocages was assembled on each Fe_3O_4/PDDA bead to form a core−satellite heteronanostructure.

The as-fabricated Fe_3O_4 beads and Fe_3O_4@Ag−Pd hybrid particles were found to be catalytically active toward the electrochemical reduction of thionine (Figure 1D), a redox dye widely used for the generation of electrochemical signals.[27] The cyclic voltammogram (CV) of a bare glassy carbon electrode (GCE) exhibited a pair of well-defined redox peaks at −0.193 and −0.160 V vs SCE, indicating a reversible two-electron redox process. With the Fe_3O_4-bead-modified GCE (GCE/Fe_3O_4), the cathodic peak current (i_{pc}) significantly increased, and the peak potential shifted by ∼−30 mV while the anodic peak current (i_{pa}) remained almost unchanged. This indicated that Fe_3O_4 efficiently catalyzed the electrochemical reduction of thionine into leucothionine, similar to the well-studied HRP/H_2O_2 system.[10−14,27] The attachment of Ag−Pd nanocages to Fe_3O_4 (GCE/Fe_3O_4@Ag−Pd) resulted in further amplification of the catalytic cathodic current by a factor of ∼5 without any further shift in the peak potential. The Fe_3O_4 beads and Fe_3O_4@Pd−Ag nanohybrids also exhibited similar electrocatalytic and signal-amplifying behaviors to methylene blue (Figure S3).

The Fe_3O_4 beads preserved their electrocatalytic activity well over multiple CV scans (Figure 2A). During each scan, the Fe_3O_4-modified GCE was exposed to freshly prepared phosphate-buffered saline (PBS) containing 25 μM thionine at pH 7.0. The robustness of the electrocatalytic performance can be interpreted as a result of the structural stability of Fe_3O_4 beads. TEM (Figure 2B,C), powder X-ray diffraction (PXRD) (Figure 2D), and Raman spectroscopy (Figure S4) measurements consistently showed that the Fe_3O_4 beads did not undergo any detectable morphological, structural, or compositional changes during the electrochemical processes and also verified that Fe_3O_4 catalyzed the electrochemical reduction of thionine rather than reacting with thionine chemically. We also recorded CVs of both bare and Fe_3O_4-modified GCEs as functions of the potential scan rate (v) (Figure S5). Linear relationships of i_{pc} and i_{pa} with $v^{1/2}$ were observed (Figure 2E), suggesting that thionine was electrocatalytically reduced on the surface of the Fe_3O_4 beads through diffusion-controlled electrode processes.[28] While the plots of i_{pa} vs $v^{1/2}$ exhibited similar slopes for the bare and Fe_3O_4-modified GCEs, the plot of i_{pc} vs $v^{1/2}$ for the Fe_3O_4-modified GCE showed a steeper slope than that of the bare GCE, further verifying the catalytic role of Fe_3O_4 in the electrochemical reduction of thionine.

The high electron conductivity, large specific surface area, and unique porous hollow geometry of the Ag−Pd bimetallic nanocages contribute synergistically to the amplification of the catalytic current. We observed that i_{pc} increased with the coverage density of Ag−Pd nanocages on the Fe_3O_4 beads (Figure S6). The role of the Ag−Pd nanocages as signal amplifiers was further verified by CV measurements on Ag−Pd-nanocage-modified GCEs (Figure S7). The Ag−Pd nanocages

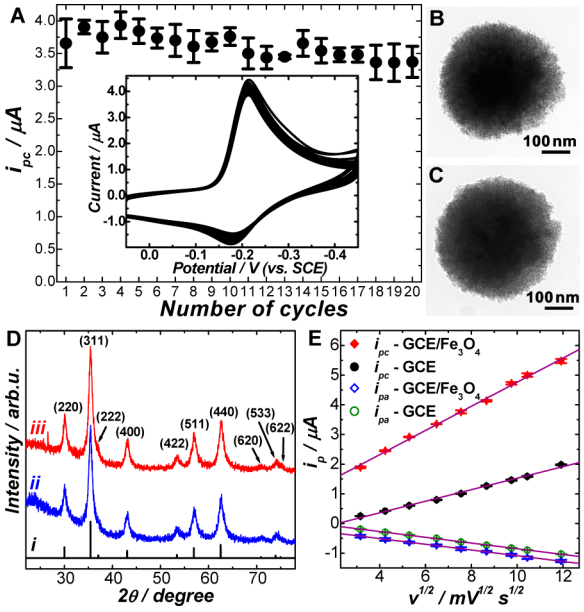

Figure 2. (A) Values of i_{pc} obtained on Fe_3O_4-modifed GCEs in 0.01 M PBS (pH 7.0) containing 25 μM thionine over 20 CV scans [scan rate (v) = 50 mV s^{-1}]. The inset shows the corresponding CVs. (B, C) TEM images of an Fe_3O_4 particle (B) before and (C) after 20 CV scans. (D) PXRD patterns of (i) bulk Fe_3O_4 and of Fe_3O_4 particles (ii) before and (iii) after 20 CV scans. (E) i_{pc} and i_{pa} as functions of $v^{1/2}$ for bare and Fe_3O_4-modifed GCEs in 25 μM thionine at pH 7.0.

amplified i_{pc} and i_{pa} simultaneously without shifting the peak potentials or the relative intensity ratio of i_{pc} and i_{pa}, indicating that the Ag−Pd nanocages themselves acted as a current amplifier rather than an electrocatalyst. The current amplification effects are also tied to the structures and compositions of the metallic nanocages. As previously demonstrated by Xia and co-workers,[25] the shell thickness and porosity of the Ag−Pd nanocages could be systematically tuned through galvanic replacement reactions. Here we observed that thinner cage shells and greater shell porosity resulted in larger signal amplification (Figure S8). To investigate the effect of the nanocage composition, Ag−Au and Ag−Pt bimetallic nanocages were synthesized through similar galvanic replacement reactions[25,29] and were subsequently tested in electrochemical reduction of thionine (Figure S9). The Fe_3O_4@Ag−Au hybrid particles exhibited much weaker i_{pc} than the Fe_3O_4@Ag−Pd hybrid particles with similar nanocage coverage. Fe_3O_4@Ag−Pt nanohybrids showed the highest i_{pc} intensity; however, much higher background currents were also observed on Fe_3O_4@Ag−Pt than on the Fe_3O_4@Ag−Pd nanohybrids.

The electrocatalytic performance of the nonenzymatic NPs was directly compared with that of the well-studied enzymatic system composed of HRP and H_2O_2.[27] In striking contrast to HRP, the Fe_3O_4-catalyzed electrochemical reduction of thionine was independent of H_2O_2. Since protons participate in the redox chemistry of thionine,[27] the redox peak currents and potentials are pH-dependent (Figure S10). As shown in Figure 3A, the HRP/H_2O_2 system generated the maximal catalytic current (Δi_p) at around pH 5 and quickly lost its catalytic activity when the pH increased to neutral and basic values. In contrast, the optimal pH for Fe_3O_4 and Fe_3O_4@Pd−Ag were around the physiologically relevant value of 7, and the particles remained their activities over a much broader pH range. To compare their thermal stabilities, we incubated HRP and the NPs at various

dx.doi.org/10.1021/ja500169y | J. Am. Chem. Soc. 2014, 136, 2288−2291

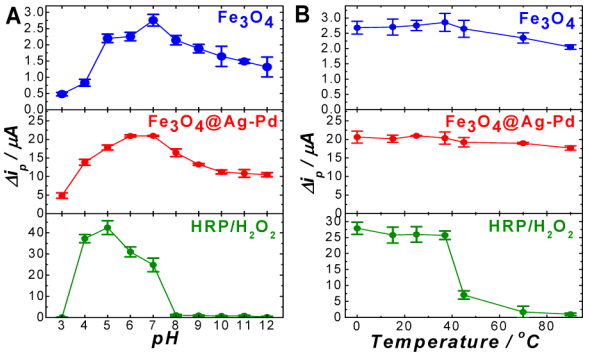

Figure 3. (A) pH dependence of and (B) effect of temperature on Δi_p obtained on Fe_3O_4-, Fe_3O_4@Ag–Pd, and HRP-modified GCEs.

temperatures for 2 h before loading them onto the GCEs and then measured their electrocatalytic activities under standard conditions (25 μM thionine, pH 7.0, 25 °C). As shown in Figure 3B, the nonenzymatic NPs were found to be stable over a wide range of temperatures from 0 to 90 °C whereas HRP quickly lost its activity as the incubation temperature became higher than 37 °C (Figure S11). The pH and temperature dependence of the peak potential shift, ΔE_p, also showed that the nonenzymatic NPs had much more robust electrocatalytic activities than the natural enzyme HRP (Figure S12). The Fe_3O_4@Ag–Pd hybrid particles exhibited long-term stability of their catalytic activity when stored at 4 °C in water (Figure S13).

The nonenzymatic hybrid NPs can be used as signal-amplifying nanoprobes for electrochemical cytosensing of low-abundance cancer cells, such as circulating tumor cells (CTCs). CTCs play crucial roles in the metastasis process[30] and are valuable biomarkers for early cancer diagnosis.[31,32] However, CTC detection has been a significant challenge because of their low abundance (1–10 CTCs per 1 billion blood cells).[33] Here we show that our electrochemical sensing approach has the sensitivity to detect just 4–5 CTCs captured on each electrode. Figure 4A schematically illustrates the major steps involved in the cytosensor assembly process. We first modified the GCE surface with a submonolayer of ~13 nm Au NPs. Then thiolated cell-targeting aptamers, SYL3C–SH,[34] were conjugated to the Au NPs on the electrode through Au–thiol interactions to create a biocompatible interface for capture of CTCs. SYL3C aptamers specifically recognize the epithelial cell adhesion molecule (EpCAM), which is overexpressed on the surfaces of most CTCs.[34] The nonspecific cell-binding sites were effectively blocked using 6-mercapto-1-hexanol (MCH). The thiolated SYL3C aptamers could also be conjugated to the Ag–Pd nanocages through metal–thiol interactions to form aptamer-functionalized hybrid nanoprobes, SYL3C–Fe_3O_4@Ag–Pd. After the targeting cells were captured on the electrode, the hybrid nanoprobes were further tethered to the surfaces of the captured cells through EpCAM–SYL3C interactions. In this way, a sandwichlike superstructure was assembled with the CTCs of interest sandwiched between the electrode interface and the nanoprobes. Figure 4B shows the evolution of differential pulse voltammetry (DPV) responses to 25 μM thionine in 0.01 M PBS (pH 7.0) during the cytosensor assembly process. The peak current decreased sequentially during the stepwise immobilization of SYL3C, MCH, and cells onto the Au-NP-modified GCE because of the insulating properties of these biomolecules and cells. However, after the nanoprobes were attached to the captured cell surfaces, the DPV curve showed a sharp current

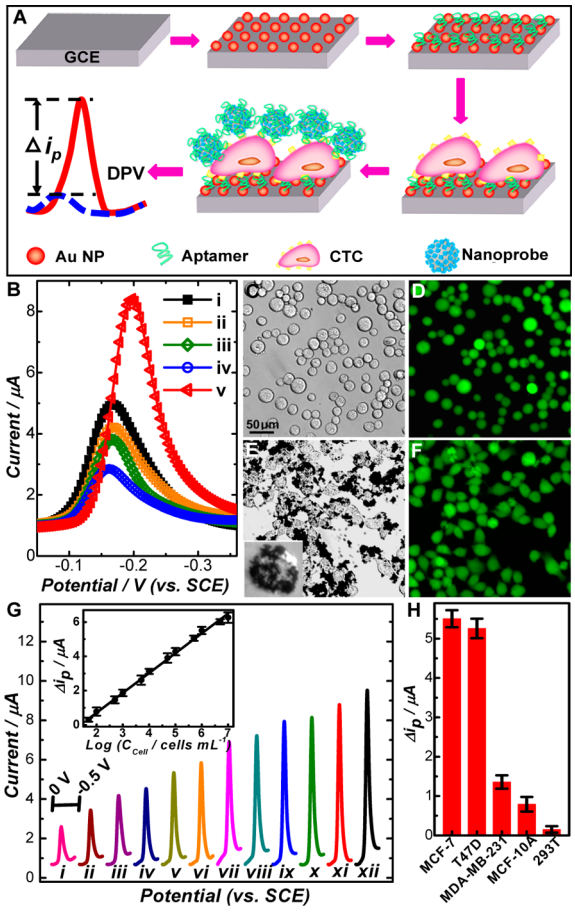

Figure 4. (A) Schematic illustration of the cytosensor assembly process. (B) DPV responses to 25 μM thionine in 0.01 M PBS (pH 7.0) on (i) Au/GCE, (ii) SYL3C/Au/GCE, (iii) MCH/SYL3C/Au/GCE, (iv) MCF-7/MCH/SYL3C/Au/GCE, and (v) nanoprobes/MCF-7/MCH/SYL3C/Au/GCE. (C) Bright-field optical and (D) fluorescence microscopy images of calcein-AM-stained MCF-7 cells after they were captured on the electrode surface for 1 h. (E) Optical and (F) fluorescence microscopy images of calcein-AM-stained, surface-captured MCF-7 cells after incubation with nanoprobes for 1 h. The inset in (E) shows an optical microscopy image of one MCF-7 cell with nanoprobes attached to the cell surface. All of the images share the scale bar in (C). (G) DPV responses to different concentrations of MCF-7 cells (from i to xii: 50, 1×10^2, 5×10^2, 1×10^3, 5×10^3, 1×10^4, 5×10^4, 1×10^5, 5×10^5, 1×10^6, 5×10^6, and 1×10^7 cells mL^{-1}). The inset shows a plot of Δi_p vs the logarithm of the MCF-7 cell concentration. (H) DPV responses (Δi_p) to various types of cells at a concentration of 1×10^6 cells mL^{-1}.

increase and a potential shift due to the electrocatalytic and signal-amplifying capabilities of the nanoprobes. The increase in the DPV signal, Δi_p, was determined by the total number of nanoprobes attached to the captured cells.

The cell-adhesion specificity and viability were characterized through microscopy imaging. We chose MCF-7 and T47D as models for CTCs because of their high levels of EpCAM expression, MB-MDA-231 and MCF-10A as control cells with low EpCAM expression levels, and human embryonic kidney (HEK) 293T cells as the EpCAM-negative control.[35] The efficiencies of cell capture and nanoprobe attachment both increased with the EpCAM expression level of various types of cells (Figure 4C,E and Figure S14). To visualize the cell viability, we stained the captured cells with calcein acetoxymethyl ester (calcein-AM), a widely used cell viability indicator, before and

dx.doi.org/10.1021/ja500169y | J. Am. Chem. Soc. 2014, 136, 2288–2291

after nanoprobe attachment. The strong fluorescence signals from the cells indicated that the cells were alive during the cytosensing processes (Figure 4D,F).

The sensitivity and linear response range of the cytosensors were evaluated using MCF-7 and T47D as the model cells. As shown in Figure 4G and Figure S15, the DPV peak currents increased with increasing cell concentration. The calibration curves for both types of cells displayed a linear relationship between Δi_p and the logarithm of the cell concentration over the range of 50 to 1×10^7 cells mL^{-1} with a correlation coefficient of 0.998 ($n = 12$). The detection limits for MCF-7 and T47D cells were determined to be ~34 and ~42 cells mL^{-1} at 3σ. As 100 μL of cell suspension was used for incubation, our approach achieved detection limits of ~4 MCF-7 and ~5 T47D cells, which are significantly lower than those of other electrochemical cytosensing approaches based on enzymatic signal amplification,[11,14,36] electrochemical impedance spectroscopy,[37] and electrochemiluminescence.[38] This electrochemical cytosensing approach is capable of differentiating the EpCAM expression levels in different types of cells and identifying the CTCs with high EpCAM expression from low- or non-EpCAM-expressing cells (see Figure 4H).

In summary, we have discovered a new function of Fe_3O_4 NPs as efficient electrocatalysts for the reduction of small dye molecules. Fe_3O_4@nanocage core−satellite nanohybrids combine the electrocatalysis with efficient signal amplification and exhibit significantly more robust electrocatalytic activities than the enzymatic peroxidase/H_2O_2 system. Using breast cancer cell lines as the model CTCs, we have further demonstrated the utilization of these hybrid nanoelectrocatalysts as signal-amplifying nanoprobes for ultrasensitive electrochemical cytosensing. By functionalization of the nanohybrids with other cell-targeting aptamers or antibodies, this electrochemical approach may be readily extended to the cytosensing of other types of cancer cells.

■ ASSOCIATED CONTENT

Supporting Information

Experimental details and additional figures. This material is available free of charge via the Internet at http://pubs.acs.org.

■ AUTHOR INFORMATION

Corresponding Authors

jjzhu@nju.edu.cn
wang344@mailbox.sc.edu

Notes

The authors declare no competing financial interest.

■ ACKNOWLEDGMENTS

H.W. acknowledges support through an NSF CAREER Award (DMR-1253231) and USC Startup Funds. Q.W. acknowledges support by NSF CHE-1307319. J.-J.Z. acknowledges support from the National Basic Research Program of China (2011CB933502) and NNSFC (21335004 and 21121091). T.Z. was partially supported by the Overseas Visiting Student Fellowship provided by the Chinese Scholarship Council.

■ REFERENCES

(1) Rolison, D. R. *Science* **2003**, *299*, 1698.
(2) Cracknell, J. A.; Vincent, K. A.; Armstrong, F. A. *Chem. Rev.* **2008**, *108*, 2439.
(3) Shao, Y. Y.; Wang, J.; Wu, H.; Liu, J.; Aksay, I. A.; Lin, Y. H. *Electroanalysis* **2010**, *22*, 1027.
(4) Pelossof, G.; Tel-Vered, R.; Elbaz, J.; Willner, I. *Anal. Chem.* **2010**, *82*, 4396.
(5) Wu, J. B.; Yang, H. *Acc. Chem. Res.* **2013**, *46*, 1848.
(6) Chen, J. Y.; Lim, B.; Lee, E. P.; Xia, Y. N. *Nano Today* **2009**, *4*, 81.
(7) Zheng, Y.; Jiao, Y.; Jaroniec, M.; Jin, Y. G.; Qiao, S. Z. *Small* **2012**, *8*, 3550.
(8) Joo, S. H.; Choi, S. J.; Oh, I.; Kwak, J.; Liu, Z.; Terasaki, O.; Ryoo, R. *Nature* **2001**, *412*, 169.
(9) Wildgoose, G. G.; Banks, C. E.; Compton, R. G. *Small* **2006**, *2*, 182.
(10) Du, D.; Zou, Z. X.; Shin, Y. S.; Wang, J.; Wu, H.; Engelhard, M. H.; Liu, J.; Aksay, I. A.; Lin, Y. H. *Anal. Chem.* **2010**, *82*, 2989.
(11) Zheng, T. T.; Tan, T. T.; Zhang, Q. F.; Fu, J. J.; Wu, J. J.; Zhang, K.; Zhu, J. J.; Wang, H. *Nanoscale* **2013**, *5*, 10360.
(12) Mani, V.; Chikkaveeraiah, B. V.; Patel, V.; Gutkind, J. S.; Rusling, J. F. *ACS Nano* **2009**, *3*, 585.
(13) Yu, X.; Munge, B.; Patel, V.; Jensen, G.; Bhirde, A.; Gong, J. D.; Kim, S. N.; Gillespie, J.; Gutkind, J. S.; Papadimitrakopoulos, F.; Rusling, J. F. *J. Am. Chem. Soc.* **2006**, *128*, 11199.
(14) Zhang, J. J.; Cheng, F. F.; Zheng, T. T.; Zhu, J. J. *Anal. Chem.* **2010**, *82*, 3547.
(15) Bourdillon, C.; Demaille, C.; Gueris, J.; Moiroux, J.; Savéant, J.-M. *J. Am. Chem. Soc.* **1993**, *115*, 12264.
(16) Xiao, Y.; Patolsky, F.; Katz, E.; Hainfeld, J. F.; Willner, I. *Science* **2003**, *299*, 1877.
(17) Wang, J.; Liu, G. D.; Jan, M. R. *J. Am. Chem. Soc.* **2004**, *126*, 3010.
(18) Pankhurst, Q. A.; Connolly, J.; Jones, S. K.; Dobson, J. *J. Phys. D: Appl. Phys.* **2003**, *36*, R167.
(19) Gao, L. Z.; Zhuang, J.; Nie, L.; Zhang, J. B.; Zhang, Y.; Gu, N.; Wang, T. H.; Feng, J.; Yang, D. L.; Perrett, S.; Yan, X. *Nat. Nanotechnol.* **2007**, *2*, 577.
(20) Chen, Z. W.; Yin, J. J.; Zhou, Y. T.; Zhang, Y.; Song, L.; Song, M. J.; Hu, S. L.; Gu, N. *ACS Nano* **2012**, *6*, 4001.
(21) Zhang, X. Q.; Gong, S. W.; Zhang, Y.; Yang, T.; Wang, C. Y.; Gu, N. *J. Mater. Chem.* **2010**, *20*, 5110.
(22) Zhang, L. H.; Zhai, Y. M.; Gao, N.; Wen, D.; Dong, S. J. *Electrochem. Commun.* **2008**, *10*, 1524.
(23) Sun, X. L.; Guo, S. J.; Liu, Y.; Sun, S. H. *Nano Lett.* **2012**, *12*, 4859.
(24) Xia, X. H.; Zeng, J.; Oetjen, L. K.; Li, Q. G.; Xia, Y. N. *J. Am. Chem. Soc.* **2012**, *134*, 1793.
(25) Chen, J. Y.; Wiley, B.; McLellan, J.; Xiong, Y. J.; Li, Z. Y.; Xia, Y. N. *Nano Lett.* **2005**, *5*, 2058.
(26) Liu, S. H.; Lu, F.; Jia, X. D.; Cheng, F. F.; Jiang, L. P.; Zhu, J. J. *CrystEngComm* **2011**, *13*, 2425.
(27) Ruan, C.; Yang, F.; Lei, C.; Deng, J. Q. *Anal. Chem.* **1998**, *70*, 1721.
(28) Bard, A. J.; Faulkner, L. R. *Electrochemical Methods: Fundamentals and Applications*; Wiley: New York, 2001.
(29) Skrabalak, S. E.; Au, L.; Li, X. D.; Xia, Y. N. *Nat. Protoc.* **2007**, *2*, 2182.
(30) Pantel, K.; Brakenhoff, R. H.; Brandt, B. *Nat. Rev. Cancer* **2008**, *8*, 329.
(31) Nakagawa, T.; Martinez, S. R.; Goto, Y.; Koyanagi, K.; Kitago, M.; Shingai, T.; Elashoff, D. A.; Ye, X.; Singer, F. R.; Giuliano, A. E.; Hoon, D. S. B. *Clin. Cancer Res.* **2007**, *13*, 4105.
(32) Aurilio, G.; Sciandivasci, A.; Munzone, E.; Sandri, M. T.; Zorzino, L.; Cassatella, M. C.; Verri, E.; Rocca, M. C.; Nole, F. *Expert Rev. Anticancer Ther.* **2012**, *12*, 203.
(33) Paterlini-Brechot, P.; Benali, N. L. *Cancer Lett.* **2007**, *253*, 180.
(34) Song, Y. L.; Zhu, Z.; An, Y.; Zhang, W. T.; Zhang, H. M.; Liu, D.; Yu, C. D.; Duan, W.; Yang, C. J. *Anal. Chem.* **2013**, *85*, 4141.
(35) Martowicz, A.; Spizzo, G.; Gastl, G.; Untergasser, G. *BMC Cancer* **2012**, *12*, 501.
(36) Ding, L.; Ji, Q. J.; Qian, R. C.; Cheng, W.; Ju, H. X. *Anal. Chem.* **2010**, *82*, 1292.
(37) Hao, C.; Ding, L.; Zhang, X.; Ju, H. X. *Anal. Chem.* **2007**, *79*, 4442.
(38) Wu, Y. F.; Zhou, H.; Wei, W.; Hua, X.; Wang, L. X.; Zhou, Z. X.; Liu, S. Q. *Anal. Chem.* **2012**, *84*, 1894.